SIAM J. SCI. COMPUT.
Vol. 25, No. 3, pp. 767–791

CENTRAL SCHEMES FOR MULTIDIMENSIONAL HAMILTON–JACOBI EQUATIONS*

STEVE BRYSON† AND DORON LEVY‡

Abstract. We present new, efficient central schemes for multidimensional Hamilton–Jacobi equations. These nonoscillatory, nonstaggered schemes are first- and second-order accurate and are designed to scale well with an increasing dimension. Efficiency is obtained by carefully choosing the location of the evolution points and by using a one-dimensional projection step. First- and second-order accuracy is verified for a variety of multidimensional, convex, and nonconvex problems.

Key words. Hamilton–Jacobi equations, central schemes, high resolution

AMS subject classifications. Primary, 65M06; Secondary, 35L99

DOI. 10.1137/S1064827501394969

1. Introduction. In this work we consider numerical approximations for solutions of multidimensional Hamilton–Jacobi (HJ) equations of the form

$$\frac{\partial \phi(\vec{x},t)}{\partial t} + H(\vec{x},\phi,\nabla\phi) = 0, \qquad \vec{x} \in \mathbb{R}^n, \tag{1.1}$$

subject to the initial data $\phi(\vec{x}, t=0) = \phi_0(\vec{x})$.

Hamilton–Jacobi equations are of special interest in a variety of applications, e.g., optimal control theory, image processing, geometric optics, differential games, and the calculus of variations. When the Hamiltonian does not depend on ϕ, solutions for (1.1) with smooth initial data will typically remain continuous but will develop discontinuous derivatives in finite time. Such solutions are not unique, and therefore a mechanism is required for singling out a "physically relevant solution," the *viscosity solution*. For convex Hamiltonians the viscosity solution coincides with the limit solution obtained by the vanishing viscosity method [11]. Extensions to general Hamiltonians were introduced by Crandall and Lions in [7] and have been systematically studied thereafter in a series of works [3, 5, 6, 26, 27].

Hamilton–Jacobi equations are closely related to hyperbolic conservation laws. Yet while the literature on numerical methods for conservation laws is flourishing, very little attention is given to numerical methods for HJ equations. This is surprising, given their increasing role in different applications. Crandall and Lions introduced in [8] first-order numerical approximations to the viscosity solution of a simplified version of (1.1), with a Hamiltonian that depends only on the derivative of ϕ. Extensions to more general Hamiltonians are due to Souganidis [37]. Discontinuous Galerkin (DG) methods for HJ equations were introduced in [10, 23]. Multidimensional DG schemes

*Received by the editors August 2, 2001; accepted for publication (in revised form) April 15, 2002; published electronically November 21, 2003.

http://www.siam.org/journals/sisc/25-3/39496.html

†Program in Scientific Computing and Computational Mathematics, Stanford University, Stanford, CA 94305-3125 (bryson@sccm.stanford.edu), and NASA Advanced Supercomputing Division, NASA Ames Research Center, Moffett Field, CA 94035-1000 (bryson@nas.nasa.gov).

‡Department of Mathematics, Stanford University, Stanford, CA 94305-2125 (dlevy@math.stanford.edu). The research of this author was supported in part by the National Science Foundation under Career Grant DMS-0133511.

are based on transforming a scalar equation into a weakly hyperbolic system which is over- or underdetermined; hence an additional least-squares step is required to single out a solution. High-order Godunov-type methods were introduced in [33, 34] (see also [35]). and were based on an essentially nonoscillatory (ENO) reconstruction step that was evolved in time with a first-order monotone flux. Schemes on unstructured grids were derived in [1] and [39] based on [14]. The least dissipative flux, the Godunov flux, requires solving Riemann problems at cell interfaces. Central schemes avoid these difficulties by evolving the solution in smooth regions, i.e., by averaging over discontinuities. Such schemes have been widely studied for conservation laws, the prototype being the first-order Lax–Friedrichs (LxF) scheme [9]. A one-dimensional second-order extension is due to Nessyahu and Tadmor [32]. Central schemes do not require Riemann solvers, which makes them suitable for solving systems of equations and for multidimensional problems. Extensions to two space dimensions were done in [2, 15]; high-order central schemes were developed in [4, 24, 25, 29]; semidiscrete schemes that reduced the numerical dissipation and eliminated the staggering were developed in [17, 18, 20].

Godunov-type central schemes have recently been extended to the HJ equations in [31], which applied the first- and second-order staggered central schemes of [15, 32] to HJ equations in one and two space dimensions. L^1 convergence of order one for this scheme was proved in [30]. In [19], a second-order semidiscrete scheme was presented, following the techniques for hyperbolic conservation laws [17, 20]. While less dissipative, this scheme requires the estimation of the local speed of propagation, which is computationally intensive, in particular in multidimensional problems. In a later work [18] the numerical viscosity was further reduced by computing more precise information about local speeds of propagation.

In this paper we derive nonstaggered fully discrete central schemes for approximating solutions of (1.1). These methods combine the ideas of [19, 31] with several additional ingredients. Our scheme is presented as an n-dimensional algorithm which is designed with special consideration to performance and scaling to higher dimensions. We develop both first- and second-order accurate schemes. These schemes are based on a projection step similar to that in [12], which is one-dimensional regardless of the dimension of the problem. The methods described in this paper can also be thought of as the first step toward higher-order schemes, which is the subject of a forthcoming paper.

This paper is organized as follows. In section 2 we develop our first- and second-order scheme in one dimension. Section 3 is the heart of the paper, where we generalize these schemes to n dimensions, first introducing a multi-index notation, then deriving the location of the evolution points, and finally presenting the algorithm. Section 4 presents various examples demonstrating the first- and second-order convergence of these schemes.

2. The one-dimensional scheme. Consider the one-dimensional HJ equation

$$\phi_t + H(\phi_x) = 0 \tag{2.1}$$

subject to the initial data $\phi(x, t=0) = \phi_0(x)$. In order to approximate solutions of (2.1) we introduce a grid in space and time with mesh spacings Δx and Δt, respectively. We denote the grid points by $x_i = i\Delta x$ and $t^m = m\Delta t$ and the fixed mesh ratio by $\lambda = \Delta t/\Delta x$. Let φ_i^m denote the approximate value of $\phi(x_i, t^m)$, and $(\varphi_x)_i^m$ denote the approximate value of the derivative $\phi_x(x_i, t^m)$. We define $(\Delta\varphi)_{i+\frac{1}{2}}^m := \varphi_{i+1}^m - \varphi_i^m$.

Given φ_i^m, an approximate solution at time t^m, the approximate solution at the next time step t^{m+1}, φ_i^{m+1}, is obtained as follows:

1. *Reconstruct* a continuous piecewise-polynomial from the data, φ_i^m, and sample it at the half-integer points, $\{x_{i+1/2}\}$, to obtain the values of $\varphi_{i+\frac{1}{2}}^m$ and its derivative, $(\varphi_x)_i^m$. The order of the polynomial is related to the overall order of accuracy of the method.
2. *Evolve* $\varphi_{i+\frac{1}{2}}^m$ by solving (2.1) from time t^m to time t^{m+1}, obtaining $\varphi_{i+\frac{1}{2}}^{m+1}$. This evolution is done at the half-integer grid points, where the reconstruction is smooth, so long as the CFL condition $\lambda \left|H'\left(\varphi_x\right)\right| \leq 1/2$ is satisfied.
3. *Project* $\varphi_{i+\frac{1}{2}}^{m+1}$ back onto the integer grid points $\{x_i\}$ to get φ_i^{m+1}.

2.1. A first-order method. The derivation of the first-order method starts by reconstructing a piecewise-linear interpolant of the form

$$\varphi\left(x, t^m\right) := \sum_i \left[\varphi_i^m + \frac{(\Delta\varphi)_{i+\frac{1}{2}}^m}{\Delta x}\left(x - x_i\right)\right] \chi_{i+\frac{1}{2}}(x), \tag{2.2}$$

where $\chi_{i+\frac{1}{2}}(x)$ is the characteristic function of the interval $[x_i, x_{i+1})$. The values of the interpolant (2.2) and its derivative at the half-integer grid points, $x_{i\pm\frac{1}{2}}$, are

$$\varphi_{i\pm\frac{1}{2}}^m = \varphi_i^m \pm \frac{1}{2}\left(\Delta\varphi\right)_{i\pm\frac{1}{2}}^m, \qquad \left(\varphi_x\right)_{i\pm\frac{1}{2}}^m = \frac{(\Delta\varphi)_{i\pm\frac{1}{2}}^m}{\Delta x}.$$

Integrating (2.1) in time from t^m to t^{m+1} at $x_{i\pm\frac{1}{2}}$ and approximating the time integral with a first-order quadrature gives

$$\varphi_{i\pm\frac{1}{2}}^{m+1} = \varphi_{i\pm\frac{1}{2}}^m - \Delta t H\left(\left(\varphi_x\right)_{i\pm\frac{1}{2}}^m\right) = \varphi_i^m \pm \frac{1}{2}\left(\Delta\varphi\right)_{i\pm\frac{1}{2}}^m - \Delta t H\left(\left(\varphi_x\right)_{i\pm\frac{1}{2}}^m\right).$$

Finally, we project the evolved solution back onto the original grid points. For a first-order method it is sufficient to average $\varphi_{i\pm1/2}^{m+1}$,

$$\begin{aligned}\varphi_i^{m+1} &= \frac{\varphi_{i+\frac{1}{2}}^{m+1} + \varphi_{i-\frac{1}{2}}^{m+1}}{2} \\ &= \varphi_i^m + \frac{1}{4}\left(\left(\Delta\varphi\right)_{i+\frac{1}{2}}^m - \left(\Delta\varphi\right)_{i-\frac{1}{2}}^m\right) - \frac{\Delta t}{2}\left[H\left(\frac{\left(\Delta\varphi\right)_{i+\frac{1}{2}}^m}{\Delta x}\right) + H\left(\frac{\left(\Delta\varphi\right)_{i-\frac{1}{2}}^m}{\Delta x}\right)\right].\end{aligned} \tag{2.3}$$

The intermediate values $\varphi_{i\pm1/2}^{m+1}$ are the same as those computed in the first-order method in [32], so in one dimension we only add the projection step. This eliminates the grid staggering in [32] with little computational cost since no additional flux evaluations are required.

2.2. A second-order method. The second-order scheme is based on a piecewise-quadratic interpolant of the form

$$\varphi\left(x, t^m\right) := \sum_i \left[\varphi_i^m + \frac{(\Delta\varphi)_{i+\frac{1}{2}}^m}{\Delta x}\left(x - x_i\right) + \frac{1}{2}\frac{\mathcal{D}\left(\Delta\varphi\right)_{i+\frac{1}{2}}^m}{\left(\Delta x\right)^2}\left(x - x_i\right)\left(x - x_{i+1}\right)\right] \chi_{i+\frac{1}{2}}. \tag{2.4}$$

Here, $\mathcal{D}$ is a limiter whose goal is to prevent oscillations while maintaining the order of accuracy of the method. There are various possibilities for choosing such limiters (see [38]). One such example is the Min-Mod limiter,

$$\mathcal{D}f_i := \mathrm{MM}\left[\theta(f_{i+1}-f_i), \frac{1}{2}(f_{i+1}-f_{i-1}), \theta(f_{i+1}-f_i)\right], \qquad 1 \le \theta \le 2,$$

where the Min-Mod function is defined as

$$\mathrm{MM}\left(x_1, x_2, \ldots\right) := \begin{cases} \min_j \{x_j\} & \text{if all } x_j > 0, \\ \max_j \{x_j\} & \text{if all } x_j < 0, \\ 0 & \text{otherwise.} \end{cases}$$

Since the solution of the HJ equations (2.1) generally has a discontinuous first derivative, we follow [19] by limiting the second derivative. Limiting the discrete second derivatives was first introduced in [34] as part of the ENO limiter. With the Min-Mod limiter, the second derivative is approximated by $\mathcal{D}(\Delta\varphi)^m_{i+\frac{1}{2}}/(\Delta x)^2$, where

$$\mathcal{D}\left(\Delta\varphi\right)^m_{i+\frac{1}{2}} = \mathrm{MM}\left[\theta\left((\Delta\varphi)^m_{i+\frac{3}{2}} - (\Delta\varphi)^m_{i+\frac{1}{2}}\right), \frac{1}{2}\left((\Delta\varphi)^m_{i+\frac{3}{2}} - (\Delta\varphi)^m_{i-\frac{1}{2}}\right), \theta\left((\Delta\varphi)^m_{i+\frac{1}{2}} - (\Delta\varphi)^m_{i-\frac{1}{2}}\right)\right].$$

Sampling (2.4) and its derivative at the half-integer grid points gives

$$\varphi^m_{i\pm\frac{1}{2}} = \varphi^m_i \pm \frac{1}{2}\left(\Delta\varphi\right)^m_{i\pm\frac{1}{2}} - \frac{1}{8}\mathcal{D}\left(\Delta\varphi\right)^m_{i\pm\frac{1}{2}}, \qquad \left(\varphi_x\right)^m_{i\pm\frac{1}{2}} = \frac{(\Delta\varphi)^m_{i\pm\frac{1}{2}}}{\Delta x}.$$

We integrate (2.1) from time t^m to time t^{m+1} and approximate the time integral with a second-order midpoint quadrature

$$\int_{t^m}^{t^{m+1}} H\left(\varphi_x\left(x_{i\pm\frac{1}{2}}, t\right)\right) dt \approx \Delta t H\left(\left(\varphi_x\right)^{m+\frac{1}{2}}_{i\pm\frac{1}{2}}\right).$$

The required midvalues, $\varphi_x(x_{i\pm\frac{1}{2}}, t^{m+\frac{1}{2}})$, can be predicted using a Taylor expansion,

$$\begin{aligned}
&\varphi_x\left(x_{i\pm\frac{1}{2}}, t^{m+\frac{1}{2}}\right) = \varphi_x\left(x_{i\pm\frac{1}{2}}, t^m\right) + \frac{1}{2}\Delta t\varphi_{tx}\left(x_{i\pm\frac{1}{2}}, t^m\right) + O\left((\Delta t)^2\right) \\
&= \varphi_x\left(x_{i\pm\frac{1}{2}}, t^m\right) - \frac{1}{2}\Delta t H'\left(\varphi_x\left(x_{i\pm\frac{1}{2}}, t^m\right)\right)\varphi_{xx}\left(x_{i\pm\frac{1}{2}}, t^m\right) + O\left((\Delta t)^2\right) \\
&\approx \frac{(\Delta\varphi)^m_{i\pm\frac{1}{2}}}{\Delta x} - \frac{1}{2}\lambda H'\left(\frac{(\Delta\varphi)^m_{i\pm\frac{1}{2}}}{\Delta x}\right)\frac{\mathcal{D}\left(\Delta\varphi\right)^m_{i\pm\frac{1}{2}}}{\Delta x},
\end{aligned}$$

which leads to

$$\varphi^{m+1}_{i\pm\frac{1}{2}} = \varphi^m_{i\pm\frac{1}{2}} - \Delta t H\left(\frac{(\Delta\varphi)^m_{i\pm\frac{1}{2}}}{\Delta x} - \frac{1}{2}\lambda H'\left(\frac{(\Delta\varphi)^m_{i\pm\frac{1}{2}}}{\Delta x}\right)\frac{\mathcal{D}\left(\Delta\varphi\right)^m_{i\pm\frac{1}{2}}}{\Delta x}\right). \tag{2.5}$$

Finally, we project (2.5) back onto the integer grid points using a quadratic interpolant

$$\begin{aligned}
\varphi^{m+1}_i &= \varphi^{m+1}_{i-\frac{1}{2}} + \frac{(\Delta\varphi)^{m+1}_i}{\Delta x}\left(x_i - x_{i-\frac{1}{2}}\right) + \frac{1}{2}\frac{\mathcal{D}\left(\Delta\varphi\right)^{m+1}_i}{(\Delta x)^2}\left(x_i - x_{i-\frac{1}{2}}\right)\left(x_i - x_{i+\frac{1}{2}}\right) \\
&= \varphi^{m+1}_{i-\frac{1}{2}} + \frac{1}{2}\left(\Delta\varphi\right)^{m+1}_i - \frac{1}{8}\mathcal{D}\left(\Delta\varphi\right)^{m+1}_i,
\end{aligned}$$

where $(\Delta\varphi)_i^{m+1} = \varphi_{i+\frac{1}{2}}^{m+1} - \varphi_{i-\frac{1}{2}}^{m+1}$ and

$$\mathcal{D}\,(\Delta\varphi)_i^{m+1} = \mathrm{MM}\Big[\theta\left((\Delta\varphi)_{i+1}^{m+1} - (\Delta\varphi)_i^{m+1}\right), \frac{1}{2}\left((\Delta\varphi)_{i+1}^{m+1} - (\Delta\varphi)_{i-1}^{m+1}\right), \theta\left((\Delta\varphi)_i^{m+1} - (\Delta\varphi)_{i-1}^{m+1}\right)\Big].$$

Remark. We would like to note that even in the one-dimensional scheme, there are several differences between our method and the second-order scheme in [31]. A second-order interpolant is used to reproject the evolved fields back onto the original grid points, resulting in a nonstaggered grid compared with the staggered scheme in [31]. Also, we follow [19] by applying the nonlinear slope limiters to the second derivative.

3. Generalization to n dimensions. We are concerned with approximating solutions of the n-dimensional HJ equation of the form

$$\phi_t + H(\nabla\phi) = 0, \qquad \vec{x} \in \mathbb{R}^n, \tag{3.1}$$

subject to the initial data $\phi(\vec{x}, t) = \phi_0(\vec{x})$.

In section 3.1 we introduce a multi-index notation, which allows a presentation that nicely parallels the one-dimensional case. We then compute the optimal location of the evolution points. Sections 3.2 and 3.3 develop the first- and second-order n-dimensional schemes. The first-order method in section 3.2 below applies as is to the case where the Hamiltonian H depends also on $\vec{x}$ and ϕ. We extend the second-order method of section 3.3 to this more general case in a remark.

3.1. Preliminaries.

A multi-index notation. We define the multi-index $\alpha = (\alpha_1, \alpha_2, \ldots, \alpha_n)$ and denote by x_α the point $x_\alpha = (x_{\alpha_1}^{(1)}, x_{\alpha_2}^{(2)}, \ldots, x_{\alpha_n}^{(n)}) \in \mathbb{R}^n$. Here $x^{(k)}$ denotes the kth coordinate of x so $x_{\alpha_k}^{(k)} = \alpha_k \Delta x^{(k)}$. For example, in the conventional three-dimensional notation with indices i, j, and k and components (x, y, z), $\alpha = (i, j, k)$ and $x_\alpha = (x_i, y_j, z_k)$.

For a given α we define the special multi-indices $\alpha \pm e_k := (\alpha_1, \ldots, \alpha_k \pm 1, \ldots, \alpha_n)$, which denote an increment in the k direction. Then $\varphi_\alpha^m = \varphi(x_{\alpha_1}^{(1)}, x_{\alpha_2}^{(2)}, \ldots, x_{\alpha_n}^{(n)}; t^m)$ and $\varphi_{\alpha\pm e_k}^m = \varphi(x_{\alpha_1}^{(1)}, \ldots, x_{\alpha_k}^{(k)} \pm \Delta x^{(k)}, \ldots, x_{\alpha_n}^{(n)}; t^m)$. Finally, we denote the evolution points with the multi-indices $\pm := (\alpha_1 \pm a, \alpha_2 \pm a, \ldots, \alpha_n \pm a)$, for some constant a, so that $\varphi_\pm^m = \varphi(x_{\alpha_1}^{(1)} \pm a\Delta x^{(1)}, x_{\alpha_2}^{(2)} \pm a\Delta x^{(2)}, \ldots, x_{\alpha_n}^{(n)} \pm a\Delta x^{(n)}; t^m)$.

The location of the evolution points. We would like to determine the location of the evolution points that provides the largest stable time step. This optimal location will be as far as possible from the singularities in the solution, which occur at the boundaries of the volume defined by the grid cell faces. For simplicity we assume a grid point at the origin, $x = (0, 0, \ldots, 0)$, and scale the coordinates such that for all $k, \Delta x^{(k)} = 1$. The two evolution points will then be located at $x_\pm = (\pm a, \pm a, \ldots, \pm a)$ for a constant a that is yet to be determined.

Consider the evolution point x_+, which is at a distance $\sqrt{n}a$ from the origin. The value of φ at this point will be based on a polynomial that is constructed inside the (hyper-) volume bounded by the coordinate planes and the (hyper-) plane $\sum_{i=1}^n x^{(i)} = 1$. There will be discontinuities in the first derivative of the piecewise-polynomial interpolant $\varphi(x, t^m)$ along the sides of this hypervolume. Since we evolve

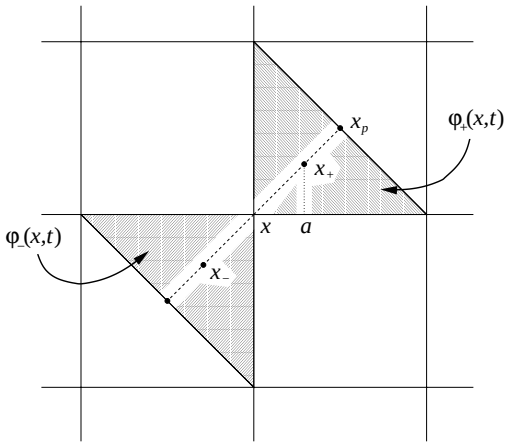

FIG. 1. *The location of the evolution points $x_\pm$ and x_p in two dimensions.*

the solution in smooth regions, an optimal choice of the evolution points is at an equidistant location from these boundaries. The diagonal line $(s, s, \ldots, s)$ (for some parameter s) intersects the (hyper-)plane $\sum_{i=1}^{n} x^{(i)} = 1$ at $s = \frac{1}{n}$, or at the point $x_p = \left(\frac{1}{n}, \frac{1}{n}, \ldots, \frac{1}{n}\right)$, which is at a distance $1/\sqrt{n}$ from the origin (see Figure 1).

The optimal choice is to require that the evolution points be equidistant from the coordinate planes and the intersection point x_p. The distance from x_+ to all the coordinate planes is a. The distance from x_+ to x_p is $1/\sqrt{n} - a\sqrt{n}$; therefore the requirement that x_+ be equidistant from the coordinate planes and x_p is

$$a = \frac{1}{n + \sqrt{n}}.$$

The evolution points in [31] were chosen as $a = 1/4$, which places them equidistant between the origin and the intersection point x_p. In n dimensions this choice generalizes to $a = (2n)^{-1}$. In our case, when $n = 2$, $a = (2 + \sqrt{2})^{-1} \approx 0.29$, which is about 15% larger than the choice $a = 1/4$. When $n = 3$, $a = (3 + \sqrt{3})^{-1} \approx 0.21$, which is about 30% larger than the choice $a = 1/6$. Thus the optimal choice of a will allow larger mesh ratios, leading to larger time steps and less dissipation.

3.2. A first-order method. For simplicity we assume that the spacing is identical in every direction, i.e., $\Delta x^{(k)} = \Delta x$ for all k. Generalization of the methods below to the case where $\Delta x^{(k)} \neq \Delta x^{(j)}$ for $k \neq j$ is not difficult: generalization of the approximation formulas below is straightforward and the optimal evolution points are found via a scaling argument. We define the forward- and backward-differences in the kth component as $\Delta_k^+ \varphi_\alpha^m := \varphi_{\alpha+e_k}^m - \varphi_\alpha^m$ and $\Delta_k^- \varphi_\alpha^m := \varphi_\alpha^m - \varphi_{\alpha-e_k}^m$, respectively. At each grid point x_α we reconstruct two linear interpolants that are valid in the two hyperquadrants that contain the points $x_\pm = x_\alpha \pm (a, \ldots, a)\Delta x$,

$$\varphi_\pm(x, t^m) := \varphi_\alpha^m + \sum_{k=1}^{n} \frac{\Delta_k^\pm \varphi_\alpha^m}{\Delta x} \left(x^{(k)} - x_{\alpha_k}^{(k)}\right). \tag{3.2}$$

In order to compute the solution at the next time step at x_α, we first compute the solution at time t^{m+1} at the evolution points $x_\pm$ and then average these two values.

The value of the linear interpolant (3.2) at $x_\pm$ is

$$\varphi(x_\pm, t^m) = \varphi_\alpha^m \pm a \sum_{k=1}^{n} \Delta_k^\pm \varphi_\alpha^m,$$

and its derivative is

$$(\nabla\varphi)_\pm^m := \left(\frac{\Delta_1^\pm \varphi_\alpha^m}{\Delta x}, \ldots, \frac{\Delta_n^\pm \varphi_\alpha^m}{\Delta x} \right).$$

Hence, the values at the evolution points $x_\pm$ at the next time step, t^{m+1}, are given by

$$\begin{aligned}\varphi(x_\pm, t^{m+1}) &= \varphi(x_\pm, t^m) - \int_{t^m}^{t^{m+1}} H\left(\nabla\varphi\left(x_\pm, t^m\right)\right) dt \approx \varphi(x_\pm, t^m) - \Delta t H\left((\nabla\varphi)_\pm^m\right) \\ &= \varphi_\alpha^m \pm a \sum_{k=1}^{n} \Delta_k^\pm \varphi_\alpha^m - \Delta t H\left(\frac{\Delta_1^\pm \varphi_\alpha^m}{\Delta x}, \ldots, \frac{\Delta_n^\pm \varphi_\alpha^m}{\Delta x} \right).\end{aligned}$$

The value at t^{m+1} at x_α is finally obtained by averaging $\varphi_\pm^{m+1} := \varphi\left(x_\pm, t^{m+1}\right)$ (compare with (2.3)),

$$\begin{aligned}\varphi_\alpha^{m+1} &= \frac{1}{2}\left(\varphi_+^{m+1} + \varphi_-^{m+1}\right) \\ &= \varphi_\alpha^m + \frac{a}{4}\left(\sum_{k=1}^{n} \Delta_k^+ \varphi_\alpha^m - \sum_{k=1}^{n} \Delta_k^- \varphi_\alpha^m \right) \\ &\quad - \frac{\Delta t}{2}\left(H\left(\frac{\Delta_1^+ \varphi_\alpha^m}{\Delta x}, \ldots, \frac{\Delta_n^+ \varphi_\alpha^m}{\Delta x} \right) + H\left(\frac{\Delta_1^- \varphi_\alpha^m}{\Delta x}, \ldots, \frac{\Delta_n^- \varphi_\alpha^m}{\Delta x} \right) \right).\end{aligned} \tag{3.3}$$

3.3. A second-order method. For simplicity we assume again that the mesh spacing is identical in every spatial direction, i.e., $\Delta x^{(k)} = \Delta x$ for all k. Similarly to the one-dimensional case in section 2.2, the n-dimensional second-order method is based on a piecewise-quadratic polynomial. For every grid node we reconstruct two n-dimensional quadratic interpolants: $\varphi_+\left(x, t^m\right)$ for the hyperquadrant along the positive diagonal, and $\varphi_-\left(x, t^m\right)$ along the negative diagonal (see Figure 1),

$$\begin{aligned}\varphi_\pm\left(x, t^m\right) &:= \varphi_\alpha^m + \sum_{k=1}^{n} \frac{\Delta_k^\pm \varphi_0^m}{\Delta x}\left(x^{(k)} - x_\alpha^{(k)}\right) \\ &+ \frac{1}{2}\sum_{k=1}^{n} \frac{\mathcal{D}_k \Delta_k^\pm \varphi_\alpha^m}{(\Delta x)^2}\left(x^{(k)} - x_\alpha^{(k)}\right)\left(x^{(k)} - x_{\alpha\pm e_k}^{(k)}\right) \\ &+ \frac{1}{2}\sum_{j=1}^{n}\sum_{\substack{k=1 \\ k\neq j}}^{n} \frac{\mathcal{D}_j \Delta_k^\pm \varphi_\alpha^m}{(\Delta x)^2}\left(x^{(j)} - x_\alpha^{(j)}\right)\left(x^{(k)} - x_\alpha^{(k)}\right).\end{aligned} \tag{3.4}$$

The Min-Mod limiter in the jth direction acting on $\Delta_k^\pm \varphi_\alpha^m$ is

$$\begin{aligned}\mathcal{D}_j \Delta_k^\pm \varphi_\alpha^m = \mathrm{MM}\Big[&\theta\left(\Delta_k^\pm \varphi_{\alpha+e_j}^m - \Delta_k^\pm \varphi_\alpha^m\right), \\ &\frac{1}{2}\left(\Delta_k^\pm \varphi_{\alpha+e_j}^m - \Delta_k^\pm \varphi_{\alpha-e_j}^m\right), \theta\left(\Delta_k^\pm \varphi_\alpha^m - \Delta_k^\pm \varphi_{\alpha-e_j}^m\right)\Big]\end{aligned}$$

so that $\mathcal{D}_j \Delta_k^\pm \varphi_\alpha^m / (\Delta x)^2$ approximates the second derivative $\partial^2 \varphi\left(x_\alpha, t^m\right) / \partial x^{(j)} \partial x^{(k)}$.

Now $x_{\pm}^{(k)} - x_{\alpha}^{(k)} = \pm a\Delta x$, $x_{+}^{(k)} - x_{\alpha+e_k}^{(k)} = (a-1)\,\Delta x$, and $x_{-}^{(k)} - x_{\alpha-e_k}^{(k)} = -(a-1)\,\Delta x$, so evaluating (3.4) at $x_{\pm}$,

$$\begin{aligned}\varphi_{\pm}^{m} &:= \varphi_{\pm}\left(x_{\pm}, t^{m}\right)\\ &= \varphi_{\alpha}^{m} \pm a\sum_{k=1}^{n}\Delta_{k}^{\pm}\varphi_{\alpha}^{m} + \frac{a\,(a-1)}{2}\sum_{k=1}^{n}\mathcal{D}_{k}\Delta_{k}^{\pm}\varphi_{\alpha}^{m} + \frac{a^{2}}{2}\sum_{j=1}^{n}\sum_{\substack{k=1\\k\neq j}}^{n}\mathcal{D}_{j}\Delta_{k}^{\pm}\varphi_{\alpha}^{m}.\end{aligned}$$

The approximation to the first derivative of (3.4) in the pth direction is given by

$$\begin{aligned}\frac{\partial\varphi_{\pm}\left(x, t^{m}\right)}{\partial x^{(p)}} \approx \frac{\Delta_{p}^{\pm}\varphi_{\alpha}^{m}}{\Delta x} + \frac{\mathcal{D}_{p}\Delta_{p}^{\pm}\varphi_{\alpha}^{m}}{2\left(\Delta x\right)^{2}}\left[\left(x_{\pm}^{(p)} - x_{\alpha}^{(p)}\right) + \left(x_{\pm}^{(p)} - x_{\alpha\pm e_p}^{(p)}\right)\right]\\ + \frac{1}{2\left(\Delta x\right)^{2}}\sum_{\substack{k=1\\k\neq p}}^{n}\left[\mathcal{D}_{p}\Delta_{k}^{\pm}\varphi_{\alpha}^{m} + \mathcal{D}_{k}\Delta_{p}^{\pm}\varphi_{\alpha}^{m}\right]\left(x_{\pm}^{(k)} - x_{\alpha}^{(k)}\right),\end{aligned}$$

which when evaluated at $x_{\pm}$ is

$$\begin{aligned}\left(\frac{\partial\varphi}{\partial x^{(p)}}\right)_{\pm}^{m} &:= \left.\frac{\partial\varphi_{\pm}\left(x, t^{m}\right)}{\partial x^{(p)}}\right|_{x_{\pm}}\\ &= \frac{\Delta_{p}^{\pm}\varphi_{\alpha}^{m}}{\Delta x} \pm \frac{2a-1}{2}\frac{\mathcal{D}_{p}\Delta_{p}^{\pm}\varphi_{\alpha}^{m}}{\Delta x} \pm \frac{a}{2}\sum_{\substack{k=1\\k\neq p}}^{n}\frac{\mathcal{D}_{p}\Delta_{k}^{\pm}\varphi_{\alpha}^{m} + \mathcal{D}_{k}\Delta_{p}^{\pm}\varphi_{\alpha}^{m}}{\Delta x}.\end{aligned}$$

The approximation to the second derivative is given by

$$\left(\frac{\partial^{2}\varphi_{\pm}}{\partial x^{(q)}\partial x^{(p)}}\right)^{m} = \frac{\mathcal{D}_{p}\Delta_{q}^{\pm}\varphi_{\alpha}^{m} + \mathcal{D}_{q}\Delta_{p}^{\pm}\varphi_{\alpha}^{m}}{2\left(\Delta x\right)^{2}}.$$

The solution at the next time step at the evolution points $\varphi_{\pm}^{m+1}$ is obtained by evolving the reconstruction (3.4) according to (3.1). The integral of the Hamiltonian is approximated by a second-order midpoint quadrature, $\int_{t^m}^{t^{m+1}} H\left(\nabla\varphi\left(x_{i\pm}, t\right)\right) dt \approx \Delta t H((\nabla\varphi)_{\pm}^{m+\frac{1}{2}})$, which at the evolution points gives

$$\varphi_{\pm}^{m+1} = \varphi_{\pm}^{m} - \Delta t H\left((\nabla\varphi)_{\pm}^{m+\frac{1}{2}}\right). \tag{3.5}$$

Here

$$(\nabla\varphi)_{\pm}^{m} := \left(\left(\frac{\partial\varphi}{\partial x^{(1)}}\right)_{\pm}^{m}, \ldots, \left(\frac{\partial\varphi}{\partial x^{(n)}}\right)_{\pm}^{m}\right)$$

denotes the approximation to the gradient at $x_{\pm}$. The midvalues in time can be estimated via the Taylor expansion using (3.1),

(3.6)

$$\begin{aligned}\frac{\partial\varphi}{\partial x^{(p)}}\left(x_{\pm}, t^{m+\frac{1}{2}}\right) &= \frac{\partial\varphi}{\partial x^{(p)}}\left(x_{\pm}, t^{m}\right) + \frac{\Delta t}{2}\frac{\partial^{2}\varphi}{\partial x^{(p)}\partial t}\left(x_{\pm}, t^{m}\right) + O\left(\Delta t^{2}\right)\\ &= \frac{\partial\varphi}{\partial x^{(p)}}\left(x_{\pm}, t^{m}\right) - \frac{\Delta t}{2}\sum_{k=1}^{n}\frac{\partial}{\partial\frac{\partial\varphi}{\partial x^{(k)}}}H\left(\nabla\varphi\left(x_{\pm}, t^{m}\right)\right)\frac{\partial^{2}\varphi}{\partial x^{(p)}\partial x^{(k)}}\left(x_{\pm}, t^{m}\right) + O\left(\Delta t^{2}\right).\end{aligned}$$

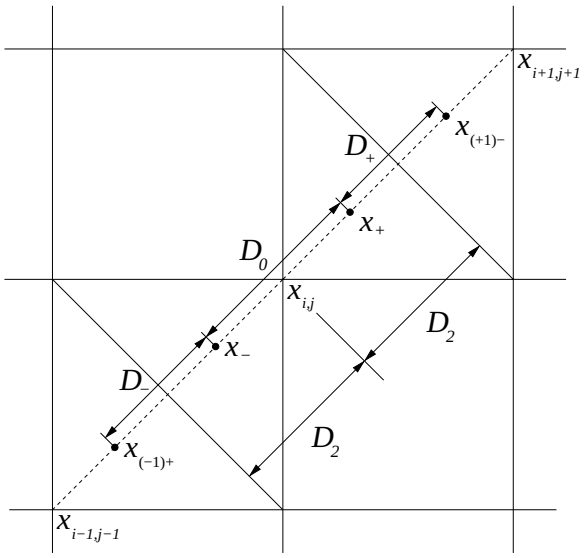

FIG. 2. *The location of the points x_+, x_-, $x_{(-1)+}$, and $x_{(+1)-}$ used in the projection step along with the distances D_0, D_+, and D_- in the two-dimensional case.*

Hence,

$$\left(\frac{\partial\varphi}{\partial x^{(p)}}\right)_{\pm}^{m+\frac{1}{2}} := \frac{\Delta_p^{\pm}\varphi_\alpha^m}{\Delta x} \pm \frac{2a-1}{2}\frac{\mathcal{D}_p\Delta_p^{\pm}\varphi_\alpha^m}{\Delta x} \pm \frac{a}{2}\sum_{\substack{k=1\\k\neq p}}^{n}\frac{\mathcal{D}_p\Delta_k^{\pm}\varphi_\alpha^m + \mathcal{D}_k\Delta_p^{\pm}\varphi_{0\alpha}^m}{\Delta x}$$

$$-\frac{\Delta t}{2}\sum_{k=1}^{n}\frac{\partial}{\partial\frac{\partial\varphi}{\partial x^k}}H\left((\nabla\varphi)_{\pm}^m\right)\frac{\mathcal{D}_p\Delta_k^{\pm}\varphi_\alpha^m + \mathcal{D}_k\Delta_p^{\pm}\varphi_\alpha^m}{2\left(\Delta x\right)^2}.$$

All that remains is to project (3.5) back onto the original grid points, x_α. This projection is one-dimensional regardless of n. We use the four evolution points x_+, x_-, $x_{(-1)+} := (x_\alpha^{(1)} - \Delta x^{(1)} + a\Delta x^{(1)}, x_\alpha^{(2)} - \Delta x^{(2)} + a\Delta x^{(2)}, \ldots, x_\alpha^{(n)} - \Delta x^{(n)} + a\Delta x^{(n)})$ and $x_{(+1)-} := (x_\alpha^{(1)} + \Delta x^{(1)} - a\Delta x^{(1)}, x_\alpha^{(2)} + \Delta x^{(2)} - a\Delta x^{(2)}, \ldots, x_\alpha^{(n)} + \Delta x^{(n)} - a\Delta x^{(n)})$ (see Figure 2). The distances between the evolution points are $D_0 := |x_+ - x_-| = 2a\sqrt{n}\Delta x$, $D_+ := |x_{(+1)-} - x_+| = (1-2a)\sqrt{n}\Delta x$, and $D_- := |x_{(-1)+} - x_-| = D_+$. We then define the approximations to the first derivative along the diagonal,

$$\frac{(d\varphi)_0^{m+1}}{D_0} := \frac{\varphi_+^{m+1} - \varphi_-^{m+1}}{D_0}, \qquad \frac{(d\varphi)_+^{m+1}}{D_+} := \frac{\varphi_{(+1)-}^{m+1} - \varphi_+^{m+1}}{D_+},$$

$$\frac{(d\varphi)_-^{m+1}}{D_-} := \frac{\varphi_-^{m+1} - \varphi_{(-1)+}^{m+1}}{D_-}.$$

The approximation to the second derivative is the limited difference $\mathcal{D}\left(d\varphi\right)_0^{m+1}/D_2$,

where $D_2 = \frac{1}{2}(D_0 + D_+)$ and

$$\mathcal{D}(d\varphi)_0^{m+1} = \mathrm{MM}\left[\theta\left(\frac{(d\varphi)_+^{m+1}}{D_+} - \frac{(d\varphi)_0^{m+1}}{D_0}\right), \frac{1}{2}\left(\frac{(d\varphi)_+^{m+1}}{D_+} - \frac{(d\varphi)_-^{m+1}}{D_-}\right), \theta\left(\frac{(d\varphi)_0^{m+1}}{D_0} - \frac{(d\varphi)_-^{m+1}}{D_-}\right)\right]. \tag{3.7}$$

The approximated value at the next time step t^{m+1} at the grid point x_α is therefore given by

$$\begin{aligned}\varphi_\alpha^{m+1} &= \varphi_-^{m+1} + \frac{(d\varphi)_0^{m+1}}{D_0}(x_\alpha - x_-) + \frac{\mathcal{D}(d\varphi)_0^{m+1}}{2D_2}(x_\alpha - x_-)(x_\alpha - x_+) \\ &= \varphi_-^{m+1} + \frac{\varphi_+^{m+1} - \varphi_-^{m+1}}{D_0}\frac{D_0}{2} - \frac{\mathcal{D}(d\varphi)_0^{m+1}}{2D_2}\frac{D_0^2}{4} \\ &= \frac{1}{2}\left(\varphi_+^{m+1} + \varphi_-^{m+1}\right) - \frac{D_0^2}{8D_2}\mathcal{D}(d\varphi)_0^{m+1},\end{aligned}$$

where $\varphi_\pm^{m+1}$ is given by (3.5) and $\mathcal{D}(d\varphi)_0^{m+1}$ is given by (3.7).

Remarks.

1. If the Hamiltonian H depends also on $\vec{x}$ and ϕ, then (3.5) becomes

$$\varphi_\pm^{m+1} = \varphi_\pm^m - \Delta t H\left(\vec{x}, \varphi_\pm^{m+\frac{1}{2}}, (\nabla\varphi)_\pm^{m+\frac{1}{2}}\right),$$

where

$$\varphi_\pm^{m+\frac{1}{2}} = \varphi_\pm^m - \frac{\Delta t}{2} H\left(\vec{x}, \varphi_\pm^m, (\nabla\varphi)_\pm^m\right),$$

and the Taylor expansion (3.6) contains the additional term

$$-\frac{\Delta t}{2}\left[\frac{\partial}{\partial x^{(p)}} H(\vec{x}, \varphi, \nabla\varphi) + \frac{\partial}{\partial \varphi} H(\vec{x}, \varphi, \nabla\varphi)\frac{\partial \varphi}{\partial x^{(p)}}\right]\Bigg|_{(x_\pm, t^m)}.$$

In this case we expect the numerical solution to be a good approximation as long as the analytical solution is continuous.

2. We would like to stress that the fully discrete scheme in [19], derived as an intermediate step in developing the semidiscrete scheme, was only first-order in time. Moreover, in two dimensions our scheme is based on only two flux evaluations per grid node compared with four flux evaluations in [18, 19]. Our scheme also does not require any estimation of the local speed of propagation at every grid point (as required in [18, 19]). The result is that our scheme is much more computationally efficient at the cost of being more dissipative. One consequence of this dissipation is that the solution of the trivial problem $H = 0$ does not remain constant, unlike in the semidiscrete formulation.
3. We wish to emphasize the advantages of the schemes presented in this paper. By avoiding staggered grids, our scheme is *simple*, *scales* well to high dimensions, and is *computationally efficient*. We show in the examples below that our second-order scheme is somewhat more accurate than that in [31]. Finally, as in all central schemes, our methods do not require the solution of any Riemann problems, so our methods can be used as black-box solvers.

We would like to summarize the second-order n-dimensional algorithm for a general Hamiltonian $H(\vec{x},\phi,\nabla\phi)$.

ALGORITHM 3.1. *Let the distance of the evolution points from the origin be* $a=\frac{1}{n+\sqrt{n}}$.

1. *For each grid node* x_α *and each* k *compute* $\Delta_k^+\varphi_\alpha^m=\varphi_{\alpha+e_k}^m-\varphi_\alpha^m$ *and* $\Delta_k^-\varphi_\alpha^m=\varphi_\alpha^m-\varphi_{\alpha-e_k}^m$.
2. *For each grid node* x_α *and for each* j *and* k *compute*

$$\mathcal{D}_j\Delta_k^\pm\varphi_\alpha^m=\mathrm{MM}\left[\theta\left(\Delta_k^\pm\varphi_{\alpha+e_j}^m-\Delta_k^\pm\varphi_\alpha^m\right),\frac{1}{2}\left(\Delta_k^\pm\varphi_{\alpha+e_j}^m-\Delta_k^\pm\varphi_{\alpha-e_j}^m\right),\theta\left(\Delta_k^\pm\varphi_\alpha^m-\Delta_k^\pm\varphi_{\alpha-e_j}^m\right)\right].$$

3. *For each grid node* x_α *compute*

$$\varphi_\pm^m=\varphi_\alpha^m\pm a\sum_{k=1}^n\Delta_k^\pm\varphi_\alpha^m+\frac{a\,(a-1)}{2}\sum_{k=1}^n\mathcal{D}_k\Delta_k^\pm\varphi_\alpha^m+\frac{a^2}{2}\sum_{j=1}^n\sum_{\substack{k=1\\k\neq j}}^n\mathcal{D}_j\Delta_k^\pm\varphi_\alpha^m,$$

and for each p *compute*

$$\left(\frac{\partial\varphi}{\partial x^{(p)}}\right)_\pm^m=\frac{\Delta_p^\pm\varphi_\alpha^m}{\Delta x}\pm\frac{2a-1}{2}\frac{\mathcal{D}_p\Delta_p^\pm\varphi_\alpha^m}{\Delta x}\pm\frac{a}{2}\sum_{\substack{k=1\\k\neq p}}^n\frac{\mathcal{D}_p\Delta_k^\pm\varphi_\alpha^m+\mathcal{D}_k\Delta_p^\pm\varphi_\alpha^m}{\Delta x},$$

$$\left(\frac{\partial\varphi}{\partial x^{(p)}}\right)_\pm^{m+\frac{1}{2}}=\left(\frac{\partial\varphi}{\partial x^{(p)}}\right)_\pm^m-\frac{\Delta t}{2}\left[\frac{\partial}{\partial x^{(p)}}H\left(\vec{x},\varphi_\pm^m,(\nabla\varphi)_\pm^m\right)+\frac{\partial}{\partial\varphi}H\left(\vec{x},\varphi_\pm^m,(\nabla\varphi)_\pm^m\right)\left(\frac{\partial\varphi}{\partial x^{(p)}}\right)_\pm^m+\sum_{k=1}^n\frac{\partial}{\partial\frac{\partial\varphi}{\partial x^k}}H\left(\vec{x},\varphi_\pm^m,(\nabla\varphi)_\pm^m\right)\left[\frac{\mathcal{D}_p\Delta_k^\pm\varphi_\alpha^m+\mathcal{D}_k\Delta_p^\pm\varphi_\alpha^m}{2\,(\Delta x)^2}\right]\right],$$

$$\varphi_{\alpha\pm}^{m+1}=\varphi_\pm^m-\Delta tH\left((\nabla\varphi)_\pm^{m+\frac{1}{2}}\right),$$

where

$$H\left((\nabla\varphi)_\pm^m\right)=H\left(\left(\frac{\partial\varphi}{\partial x^{(1)}}\right)_\pm^m,\ldots,\left(\frac{\partial\varphi}{\partial x^{(n)}}\right)_\pm^m\right).$$

4. *Let* $D_0=2a\sqrt{n}\Delta x,\ D_+=D_-=(1-2a)\sqrt{n}\Delta x$. *For each* x_α *compute*

$$\frac{(d\varphi)_0^{m+1}}{D_0}=\frac{\varphi_{\alpha+}^{m+1}-\varphi_{\alpha-}^{m+1}}{D_0},$$

$$\frac{(d\varphi)_+^{m+1}}{D_+}=\frac{\varphi_{(\alpha+1)-}^{m+1}-\varphi_{\alpha+}^{m+1}}{D_+},$$

$$\frac{(d\varphi)_-^{m+1}}{D_-}=\frac{\varphi_{\alpha-}^{m+1}-\varphi_{(\alpha-1)+}^{m+1}}{D_-}$$

(where $\alpha \pm 1$ is the multi-index $(\alpha_1 \pm 1, \ldots, \alpha_n \pm 1)$),

$$\mathcal{D}\,(d\varphi)_0^{m+1} = \mathrm{MM}\left[\theta\left(\frac{(d\varphi)_+^{m+1}}{D_+} - \frac{(d\varphi)_0^{m+1}}{D_0}\right), \frac{1}{2}\left(\frac{(d\varphi)_+^{m+1}}{D_+} - \frac{(d\varphi)_-^{m+1}}{D_-}\right), \theta\left(\frac{(d\varphi)_0^{m+1}}{D_0} - \frac{(d\varphi)_-^{m+1}}{D_-}\right)\right].$$

5. *For each x_α compute*

$$\varphi_\alpha^{m+1} = \frac{1}{2}\left(\varphi_{\alpha+}^{m+1} + \varphi_{\alpha-}^{m+1}\right) - \frac{D_0^2}{8D_2}\mathcal{D}\,(d\varphi)_0^{m+1}.$$

4. Numerical examples. We demonstrate the schemes developed in sections 2 and 3 with several examples. Some of these examples are standard test cases that can be found, e.g., in [19, 31, 34].

Example 1: A convex Hamiltonian. We start by testing the performance of our schemes on a convex Hamiltonian. We approximate solutions of the one-dimensional equation

$$\phi_t + \frac{1}{2}\left(\phi_x + 1\right)^2 = 0 \tag{4.1}$$

subject to the initial data $\phi(x,0) = -\cos(\pi x)$ and to periodic boundary conditions on $[0,2]$. The change of variables, $u\,(x,t) = \phi_x\,(x,t) + 1$, transforms the equation into the Burgers equation, $u_t + \frac{1}{2}\left(u^2\right)_x = 0$, which can be solved via the method of characteristics [34]. As is well known, the Burgers equation generally develops discontinuous solutions even with smooth initial data, and hence we expect the solutions of (4.1) to have discontinuous derivatives. In our case, the solution develops a singularity at time $t = \pi^{-2}$.

The results of our simulations are shown in Figures 3 and 4. The order of accuracy of these methods is determined from the relative L^1-error (see [30]) defined as the L^1-norm of the error divided by the L^1-norm of the exact solution. The results before the singularity, at $T = 0.8/\pi^2$, are given in Table 1, and after the singularity, at $T = 1.5/\pi^2$, in Table 2.

In two dimensions we solve a similar problem,

$$\phi_t + \frac{1}{2}\left(\phi_x + \phi_y + 1\right)^2 = 0, \tag{4.2}$$

which can be reduced to a one-dimensional problem via the coordinate transformation $\binom{\xi}{\eta} = \frac{1}{2}\left(\begin{smallmatrix}1 & 1\\ 1 & -1\end{smallmatrix}\right)\binom{x}{y}$. The results of the second-order calculations for the initial data $\phi\,(x,y,0) = -\cos\left(\pi(x+y)/2\right) = -\cos\left(\pi\xi\right)$ are shown in Figures 5–6. The convergence rates for the first- and second-order two-dimensional schemes before and after the development of the singularity are shown in Tables 3–4.

Table 5 compares the accuracy of our second-order scheme with the second-order scheme of Lin and Tadmor [31] for problem (4.2) in one and two dimensions for various N. For each algorithm, value of N, and dimension, the CFL number is chosen to minimize the relative error. We see that our second-order scheme gives errors in the range of half that of Lin and Tadmor.

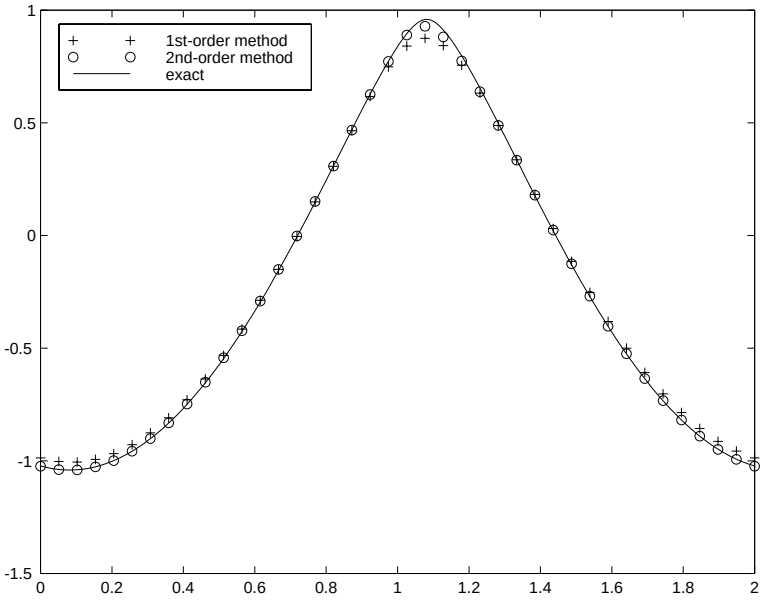

FIG. 3. *Example* 1. *The one-dimensional convex Hamiltonian* (4.1). *The solution is computed at* $T = 0.8/\pi^2$ *before the formation of singularities.* $N = 40$. *Shown are the first-order approximation, the second-order approximation, and the exact solution.*

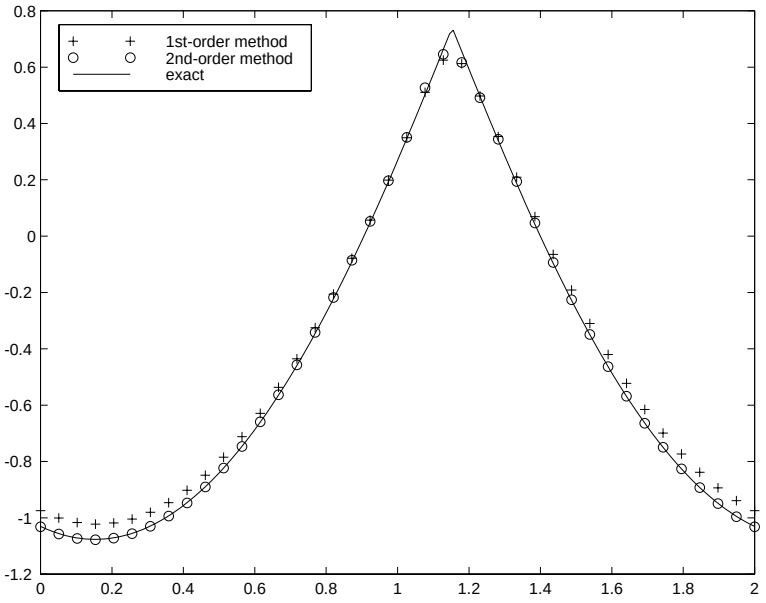

FIG. 4. *Example* 1. *The one-dimensional convex Hamiltonian* (4.1). *The solution is computed at* $T = 1.5/\pi^2$ *after the formation of singularities.* $N = 40$. *Shown are the first-order approximation, the second-order approximation, and the exact solution.*

TABLE 1

Relative L^1-errors for the one-dimensional convex HJ problem (4.1) *before the singularity formation.* $T = 0.8/\pi^2$.

	First-order method		*Second-order method*	
N	*Relative* L^1*-error*	L^1*-order*	*Relative* L^1*-error*	L^1*-order*
100	3.58×10^{-2}	–	1.38×10^{-3}	–
200	1.72×10^{-2}	1.06	3.33×10^{-4}	2.05
400	8.50×10^{-3}	1.02	8.20×10^{-5}	2.02
800	4.22×10^{-3}	1.01	2.02×10^{-5}	2.02

TABLE 2

Relative L^1-errors for the one-dimensional convex HJ problem (4.1) *after the formation of the singularity.* $T = 1.5/\pi^2$.

	First-order method		*Second-order method*	
N	*Relative* L^1*-error*	L^1*-order*	*Relative* L^1*-error*	L^1*-order*
100	5.49×10^{-2}	–	1.74×10^{-3}	–
200	2.62×10^{-2}	1.07	3.91×10^{-4}	2.15
400	1.28×10^{-2}	1.03	1.26×10^{-4}	1.63
800	6.38×10^{-3}	1.00	5.05×10^{-5}	1.32

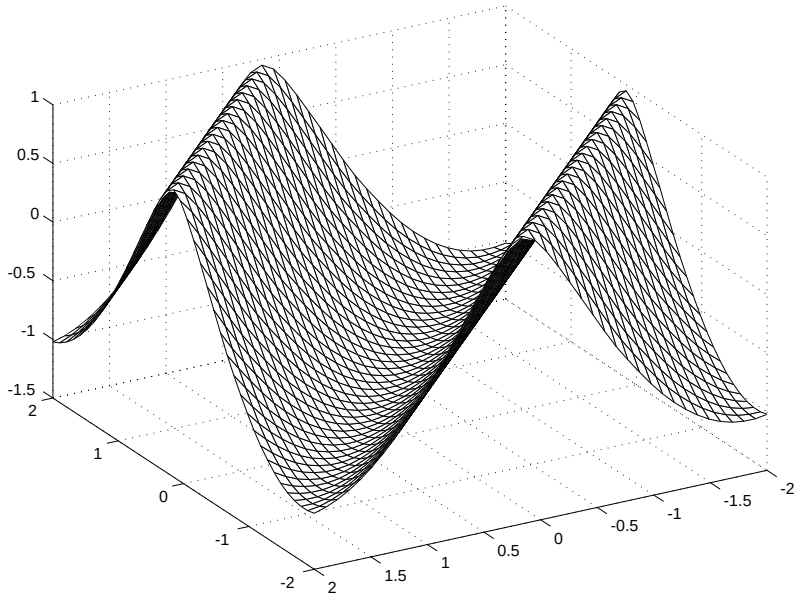

FIG. 5. *Example* 1. *The two-dimensional convex Hamiltonian* (4.2). *The solution is computed at* $T = 0.8/\pi^2$ *before the formation of singularities.* $N = 40 \times 40$.

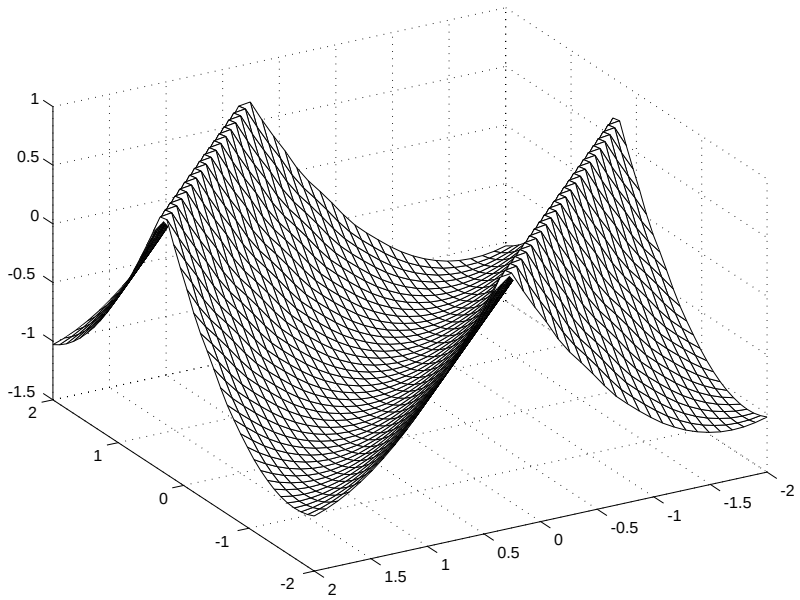

FIG. 6. *Example* 1. *The two-dimensional convex Hamiltonian* (4.2). *The solution is computed at* $T = 1.5/\pi^2$ *after the formation of singularities.* $N = 40 \times 40$.

TABLE 3

Relative L^1*-errors for the two-dimensional convex HJ problem* (4.2) *before the singularity formation.* $T = 0.8/\pi^2$.

	First-order method		*Second-order method*	
N	*Relative* L^1*-error*	L^1*-order*	*Relative* L^1*-error*	L^1*-order*
100	1.38×10^{-2}	–	6.27×10^{-4}	–
200	6.55×10^{-3}	1.07	1.41×10^{-4}	2.15
400	3.18×10^{-3}	1.04	3.32×10^{-5}	2.09
800	1.58×10^{-3}	1.01	9.89×10^{-6}	1.75

TABLE 4

Relative L^1*-errors for the two-dimensional convex HJ problem* (4.2) *after the singularity formation.* $T = 1.5/\pi^2$.

	First-order method		*Second-order method*	
N	*Relative* L^1*-error*	L^1*-order*	*Relative* L^1*-error*	L^1*-order*
100	2.02×10^{-2}	–	2.63×10^{-3}	–
200	9.82×10^{-3}	1.04	6.11×10^{-4}	2.01
400	4.89×10^{-3}	1.01	1.84×10^{-4}	1.73
800	2.44×10^{-3}	1.00	6.22×10^{-5}	1.57

TABLE 5

A comparison of the relative L^1-errors for Algorithm 3.1 *($e_{3.1}$) and the second-order algorithm of Lin and Tadmor (LT)* [31] *(e_{LT}). Two-dimensional convex HJ problem* (4.2) *before the singularity formation $T = 0.5/\pi^2$.*

	One-dimensional			*Two-dimensional*		
N	*Algorithm* 3.1	2*nd-order LT*	$e_{3.1}/e_{LT}$	*Algorithm* 3.1	2*nd-order LT*	$e_{3.1}/e_{LT}$
100	2.43×10^{-4}	4.20×10^{-4}	0.58	2.81×10^{-4}	6.38×10^{-4}	0.44
200	6.60×10^{-5}	1.07×10^{-4}	0.62	6.99×10^{-5}	1.64×10^{-4}	0.43
400	1.83×10^{-5}	3.60×10^{-5}	0.51	1.92×10^{-5}	4.20×10^{-5}	0.46
800	4.80×10^{-6}	1.13×10^{-5}	0.42	5.20×10^{-6}	1.22×10^{-5}	0.42

TABLE 6

Relative L^1-errors for the three-dimensional convex HJ problem (4.3) *before the singularity formation. $T = 0.08$.*

	First-order method		*Second-order method*	
N	*Relative L^1-error*	*L^1-order*	*Relative L^1-error*	*L^1-order*
50	4.27×10^{-2}	–	4.66×10^{-3}	–
100	2.06×10^{-2}	1.05	1.11×10^{-3}	2.07
200	1.29×10^{-2}	0.68	2.98×10^{-4}	1.89

TABLE 7

Relative L^1-errors for the three-dimensional convex HJ problem (4.3) *after the singularity formation. $T = 0.152$.*

	First-order method		*Second-order method*	
N	*Relative L^1-error*	*L^1-order*	*Relative L^1-error*	*L^1-order*
50	6.51×10^{-2}	–	5.43×10^{-3}	–
100	3.06×10^{-2}	1.09	1.23×10^{-3}	2.13
200	1.57×10^{-2}	0.96	3.98×10^{-4}	1.63

We proceed with a three-dimensional generalization of (4.2),

$$\phi_t + \frac{1}{2}\left(\phi_x + \phi_y + \phi_z + 1\right)^2 = 0, \tag{4.3}$$

subject to the initial data $\phi(x, y, 0) = -\cos(\pi(x + y + z)/3)$. The convergence results for the first- and second-order three-dimensional schemes before and after the singularity formation are given in Tables 6–7.

Example 2: A nonconvex Hamiltonian. In this example we deal with nonconvex HJ equations. In one dimension we solve

$$\phi_t - \cos(\phi_x + 1) = 0 \tag{4.4}$$

subject to the initial data $\phi(x, 0) = -\cos(\pi x)$ and periodic boundary conditions on $[0, 2]$. In this case, (4.4) has a smooth solution for $t \lesssim 1.049/\pi^2$, after which a singularity forms. A second singularity forms at $t \approx 1.29/\pi^2$. The results are shown in Figures 7–8. The convergence results before and after the singularity formation are given in Tables 8–9.

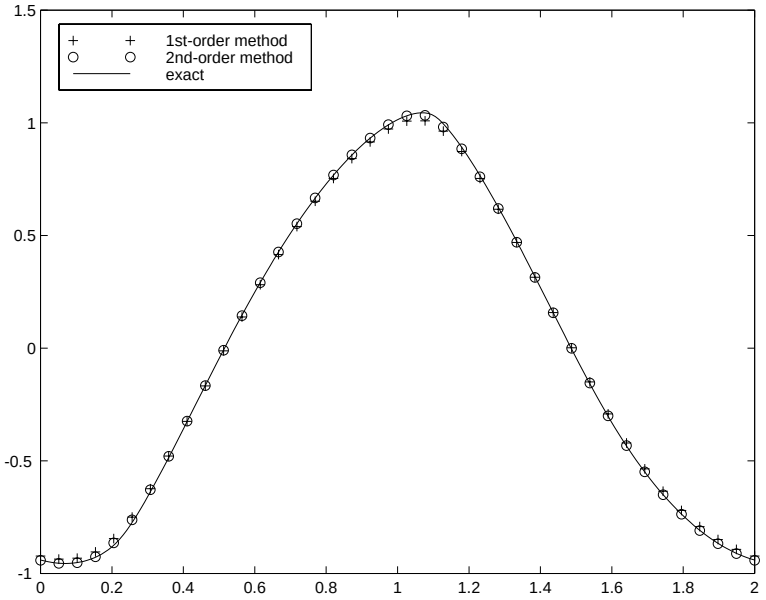

FIG. 7. *Example* 2. *The one-dimensional nonconvex Hamiltonian* (4.4). *The solution is computed at* $T = 0.8/\pi^2$ *before the formation of singularities.* $N = 40$. *Shown are the first-order approximation, the second-order approximation, and the exact solution.*

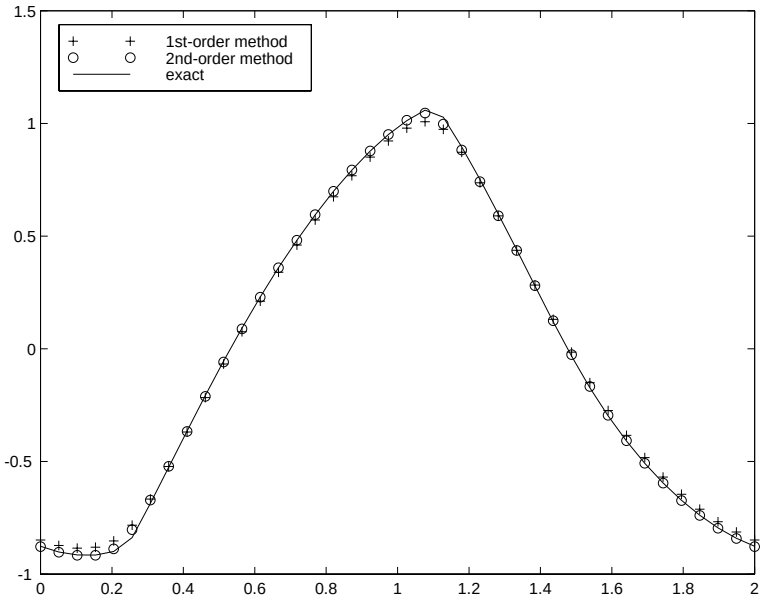

FIG. 8. *Example* 2. *The one-dimensional nonconvex Hamiltonian* (4.4). *The solution is computed at* $T = 1.5/\pi^2$ *after the formation of singularities.* $N = 40$. *Shown are the first-order approximation, the second-order approximation, and the exact solution.*

TABLE 8
Relative L^1-errors for the one-dimensional nonconvex HJ problem (4.4) *before the singularity formation.* $T = 0.8/\pi^2$.

	First-order method		*Second-order method*	
N	*Relative* L^1*-error*	L^1*-order*	*Relative* L^1*-error*	L^1*-order*
100	4.08×10^{-2}	–	1.84×10^{-3}	–
200	1.97×10^{-2}	1.05	4.59×10^{-4}	2.00
400	9.73×10^{-3}	1.02	1.15×10^{-4}	1.99
800	4.84×10^{-3}	1.01	2.87×10^{-5}	2.01

TABLE 9
Relative L^1-errors for the one-dimensional nonconvex HJ problem (4.4) *after the singularity formation.* $T = 1.5/\pi^2$.

	First-order method		*Second-order method*	
N	*Relative* L^1*-error*	L^1*-order*	*Relative* L^1*-error*	L^1*-order*
100	7.10×10^{-2}	–	3.09×10^{-3}	–
200	3.38×10^{-2}	1.07	8.48×10^{-4}	2.00
400	1.63×10^{-2}	1.05	2.07×10^{-4}	2.08
800	8.00×10^{-3}	1.03	5.62×10^{-5}	2.04

In two dimensions we solve

$$\phi_t - \cos(\phi_x + \phi_y + 1) = 0 \tag{4.5}$$

subject to the initial data $\phi(x, y, 0) = -\cos(\pi(x + y)/2)$ and periodic boundary conditions. The results are shown in Figures 9–10. The convergence results for the first- and second-order two-dimensional schemes before and after the singularity formation are given in Tables 10–11 and confirm the expected order of accuracy of our methods.

The extension of (4.5) to three dimensions reads

$$\phi_t - \cos(\phi_x + \phi_y + \phi_z + 1) = 0. \tag{4.6}$$

The initial data are taken as $\phi(x, y, 0) = -\cos(\pi(x + y + z)/3)$. The convergence rates for the first- and second-order three-dimensional schemes are given in Tables 12–13.

Example 3: A fully two-dimensional example. The above standard examples are one-dimensional along the diagonal in two and three dimensions. To check the performance of our methods on fully two-dimensional problems, we solve

$$\phi_t + \phi_x \phi_y = 0 \tag{4.7}$$

on $[-\pi, \pi] \times [-\pi, \pi]$ subject to the initial data $\phi(x, y, 0) = \sin(x) + \cos(y)$ with periodic boundary conditions. The exact solution for this problem is given implicitly by $\phi(x, y, t) = -\cos(q)\sin(r) + \sin(q) + \cos(r)$, where $x = q - t\sin(r)$ and $y = r + t\cos(q)$. This solution is smooth for $t < 1$, continuous for all t, and has discontinuous derivatives for $t \geq 1$. The results are shown in Figure 11. The convergence results for the first- and second-order two-dimensional schemes before the singularity formation are given in Table 14 and confirm the expected order of accuracy of our methods.

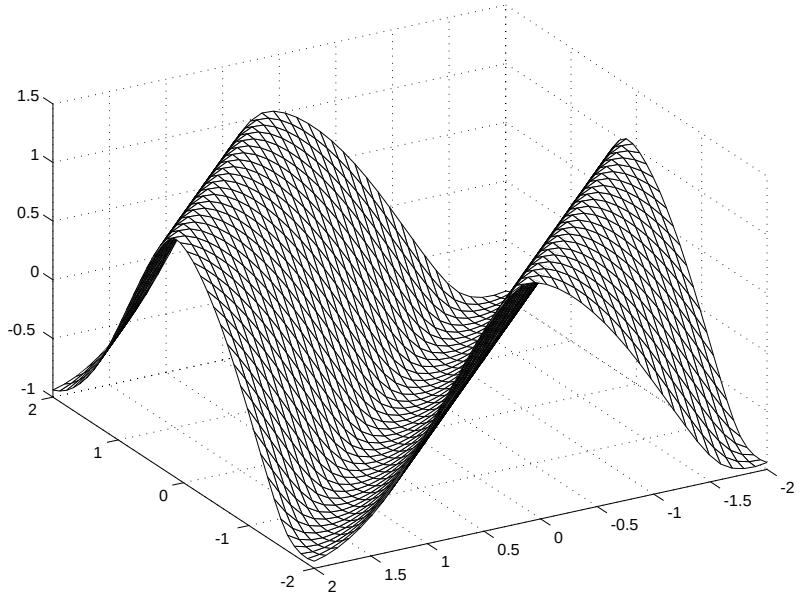

FIG. 9. *Example* 2. *The two-dimensional nonconvex Hamiltonian* (4.5). *The solution is computed at* $T = 0.8/\pi^2$ *before the formation of singularities.* $N = 40 \times 40$.

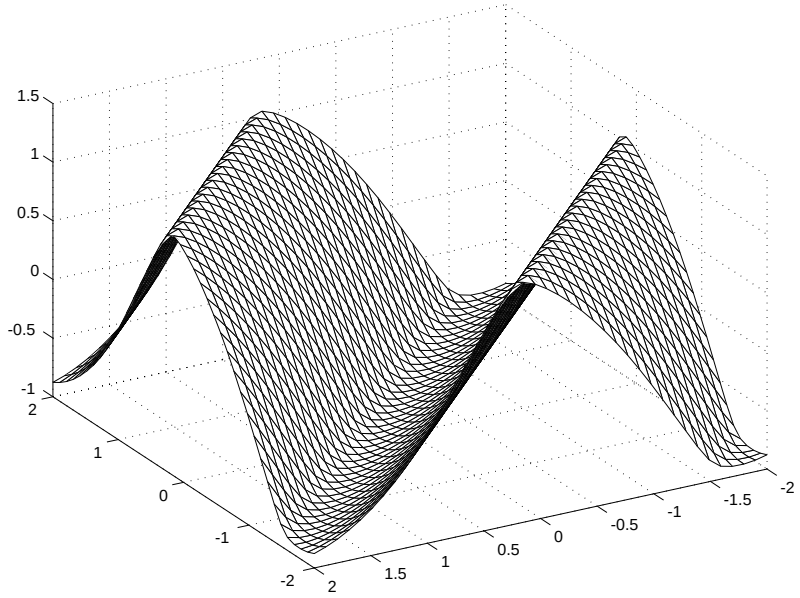

FIG. 10. *Example* 2. *The two-dimensional nonconvex Hamiltonian* (4.5). *The solution is computed at* $T = 1.5/\pi^2$ *after the formation of singularities.* $N = 40 \times 40$.

TABLE 10

Relative L^1-errors for the two-dimensional nonconvex HJ problem (4.5) *before the singularity formation.* $T = 0.8/\pi^2$.

	First-order method		*Second-order method*	
N	*Relative* L^1*-error*	L^1*-order*	*Relative* L^1*-error*	L^1*-order*
100	2.01×10^{-2}	–	1.06×10^{-3}	–
200	9.63×10^{-3}	1.06	2.54×10^{-4}	2.06
400	4.71×10^{-3}	1.03	6.15×10^{-5}	2.05
800	2.34×10^{-3}	1.01	1.52×10^{-5}	2.01

TABLE 11

Relative L^1-errors for the two-dimensional nonconvex HJ problem (4.5) *after the singularity formation.* $T = 1.5/\pi^2$.

	First-order method		*Second-order method*	
N	*Relative* L^1*-error*	L^1*-order*	*Relative* L^1*-error*	L^1*-order*
100	3.40×10^{-2}	–	2.18×10^{-3}	–
200	1.63×10^{-2}	1.06	6.02×10^{-4}	1.86
400	7.87×10^{-3}	1.05	1.47×10^{-4}	2.03
800	3.85×10^{-3}	1.03	4.18×10^{-5}	1.82

TABLE 12

Relative L^1-errors for the three-dimensional nonconvex HJ problem (4.6) *before the singularity formation.* $T = 0.08$.

	First-order method		*Second-order method*	
N	*Relative* L^1*-error*	L^1*-order*	*Relative* L^1*-error*	L^1*-order*
50	3.65×10^{-2}	–	4.21×10^{-3}	–
100	1.86×10^{-2}	0.97	1.08×10^{-3}	1.97
200	8.37×10^{-3}	1.15	2.56×10^{-4}	2.07

TABLE 13

Relative L^1-errors for the three-dimensional nonconvex HJ problem (4.6) *after the singularity formation.* $T = 0.152$.

	First-order method		*Second-order method*	
N	*Relative* L^1*-error*	L^1*-order*	*Relative* L^1*-error*	L^1*-order*
50	6.58×10^{-2}	–	7.99×10^{-3}	–
100	3.26×10^{-2}	1.01	2.23×10^{-3}	1.84
200	1.46×10^{-2}	1.16	5.65×10^{-4}	1.98

Example 4: A linear advection equation. In this example (in [13] with a misprint and corrected in [39]) we solve the one-dimensional linear advection equation; i.e., the Hamiltonian is taken as $H(\phi_x) = \phi_x$. We assume periodic boundary conditions on $[-1, 1]$, and take the initial data as $\phi(x, 0) = g(x - 0.5)$ on $[-1, 1]$, where

$$g(x) = -\left(\frac{\sqrt{3}}{2} + \frac{9}{2} + \frac{2\pi}{3}\right)(x + 1) + h(x),$$

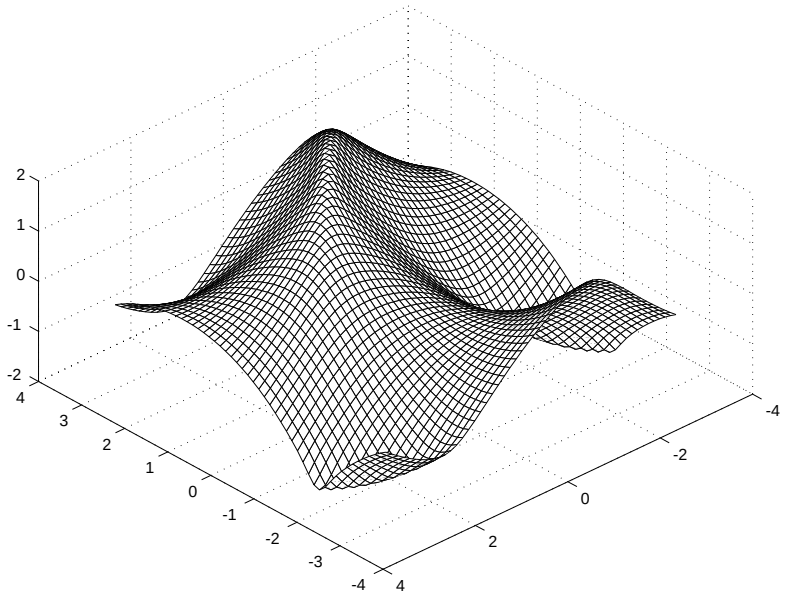

FIG. 11. *Example* 3. *The fully two-dimensional Hamiltonian* (4.7). *The solution is computed at* $T = 1.3$ *after the formation of singularities.* $N = 50 \times 50$.

TABLE 14
Relative L^1*-errors for the two-dimensional HJ problem* (4.7) *before singularity formation.* $T = 0.5$.

	First-order method		*Second-order method*	
N	*Relative* L^1*-error*	L^1*-order*	*Relative* L^1*-error*	L^1*-order*
100	3.58×10^{-3}	–	3.80×10^{-4}	–
200	1.75×10^{-3}	1.03	9.18×10^{-5}	2.05
400	8.69×10^{-4}	1.01	2.29×10^{-5}	2.00
800	4.33×10^{-4}	1.00	6.03×10^{-6}	1.92

$$h(x) = \begin{cases} 2\cos\left(\frac{3\pi}{2}x^2\right) - \sqrt{3}, & -1 < x < -\frac{1}{3}, \\ \frac{3}{2} + 3\cos(2\pi x), & -\frac{1}{3} < x < 0, \\ \frac{15}{2} - 3\cos(2\pi x), & 0 < x < \frac{1}{3}, \\ \frac{1}{3}(28 + 4\pi + \cos(3\pi x)) + 6\pi x(x-1), & \frac{1}{3} < x < 1. \end{cases}$$

The results of the second-order method are shown in Figure 12. The dissipation effects are visible in the round-off of the corners.

Example 5: Two-dimensional eikonal equation in geometric optics. We demonstrate the results obtained with the two-dimensional scheme on the nonconvex problem

$$\begin{cases} \phi_t + \sqrt{\phi_x^2 + \phi_y^2 + 1} = 0, \\ \phi(x, y, 0) = \frac{1}{4}(\cos(2\pi x) - 1)(\cos(2\pi y) - 1) - 1. \end{cases} \tag{4.8}$$

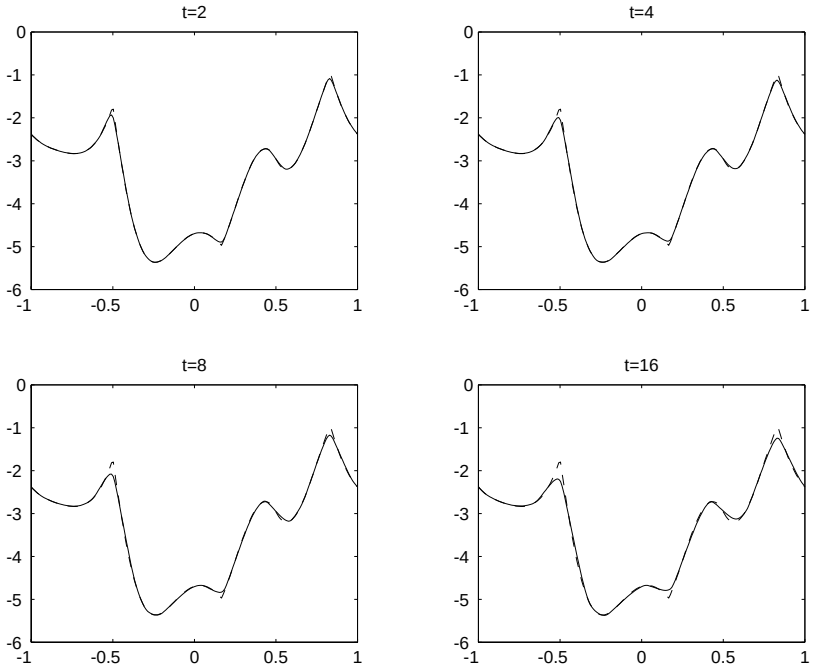

FIG. 12. *Example* 4. *A one-dimensional linear advection problem.* $N = 200$. *Solid line: approximation; dashed line: exact solution.*

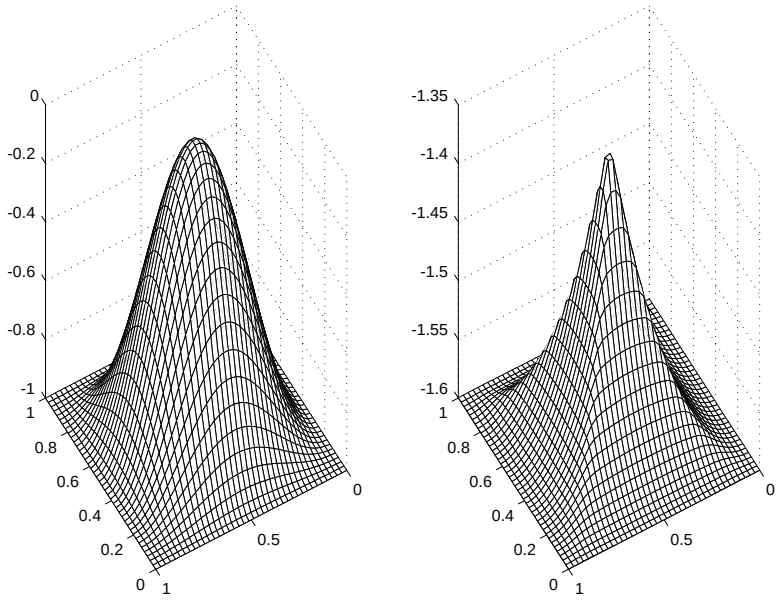

FIG. 13. *Example* 5. *The two-dimensional eikonal equation* (4.8). $N = 40 \times 40$. *Left: the initial data. Right: the solution at* $T = 0.6$.

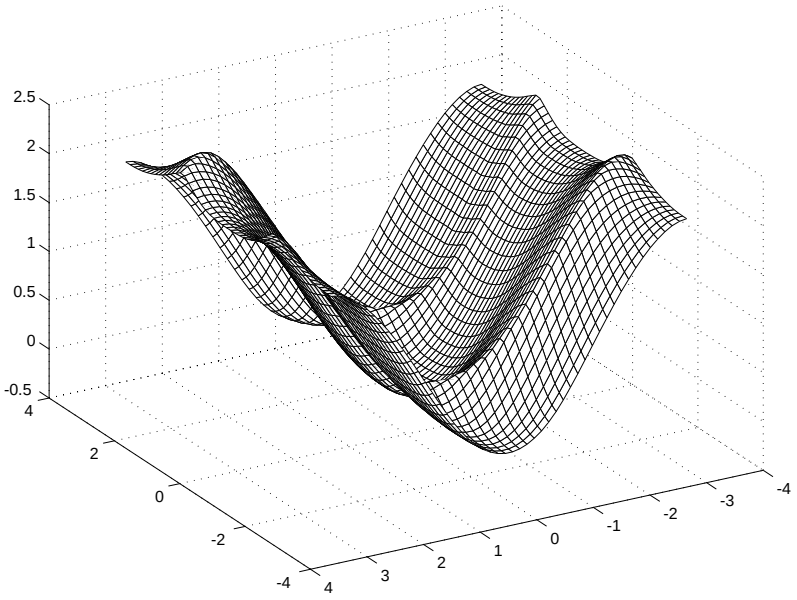

FIG. 14. *Example* 6. *The two-dimensional optimal control problem* (4.9). $T = 1$. $N = 40 \times 40$.

This model arises in geometric optics [16]. The results of our second-order method at time $T = 0.6$ are shown in Figure 13, where we see the sharp corners that develop in this problem, in agreement with the results in [31].

Example 6: Optimal control. We solve a two-dimensional problem with a more general Hamiltonian of the form $H(x, y, \nabla\phi)$. This is an optimal control problem related to cost determination [34]:

$$\text{(4.9)} \qquad \begin{cases} \phi_t - \sin(y)\,\phi_x + \sin(x)\,\phi_y + |\phi_y| - \frac{1}{2}\sin^2(y) - 1 + \cos(x) = 0, \\ \phi(x, y, 0) = 0. \end{cases}$$

This example develops a complex singularity structure. The result of our second-order scheme is in qualitative agreement with [31], as can be seen in Figure 14.

Acknowledgments. We would like to thank Ian Mitchell for helpful discussions and for suggesting the averaging strategy that is used to avoid staggering in the schemes. We thank Julie Levandosky for assistance with Example 3. We also thank Volker Elling for helpful comments on earlier drafts of this paper.

REFERENCES

[1] R. ABGRALL, *Numerical discretization of the first-order Hamilton-Jacobi equation on triangular meshes*, Comm. Pure Appl. Math., 49 (1996), pp. 1339–1373.

[2] P. ARMINJON AND M.-C. VIALLON, *Généralisation du schéma de Nessyahu-Tadmor pour une équation hyperbolique à deux dimensions d'espace*, C.R. Acad. Sci. Paris Ser. I Math., 320 (1995), pp. 85–88.

[3] G. BARLES, *Solution de Viscosité des Équations de Hamilton-Jacobi*, Springer-Verlag, Berlin, 1994.

[4] F. BIANCO, G. PUPPO, AND G. RUSSO, *High-order central schemes for hyperbolic systems of conservation laws*, SIAM J. Sci. Comput., 21 (1999), pp. 294–322.

[5] M. G. Crandall, L. C. Evans, and P.-L. Lions, *Some properties of viscosity solutions of Hamilton-Jacobi equations*, Trans. Amer. Math. Soc., 282 (1984), pp. 487–502.
[6] M. G. Crandall, H. Ishii, and P.-L. Lions, *User's guide to viscosity solutions of second order partial differential equations*, Bull. Amer. Math. Soc., 27 (1992), pp. 1–67.
[7] M. G. Crandall and P.-L. Lions, *Viscosity solutions of Hamilton-Jacobi equations*, Trans. Amer. Math. Soc., 277 (1983), pp. 1–42.
[8] M. G. Crandall and P.-L. Lions, *Two approximations of solutions of Hamilton-Jacobi equations*, Math. Comp., 43 (1984), pp. 1–19.
[9] K. O. Friedrichs and P. D. Lax, *Systems of conservation equations with a convex extension*, Proc. Natl. Acad. Sci. USA, 68 (1971), pp. 1686–1688.
[10] C. Hu and C.-W. Shu, *A discontinuous Galerkin finite element method for Hamilton–Jacobi equations*, SIAM J. Sci. Comput., 21 (1999), pp. 666–690.
[11] S. N. Kruzkov, *The Cauchy problem in the large for nonlinear equations and for certain quasilinear systems of the first order with several variables*, Soviet Math. Dokl., 5 (1964), pp. 493–496.
[12] G.-S. Jiang, D. Levy, C.-T. Lin, S. Osher, and E. Tadmor, *High-resolution nonoscillatory central schemes with nonstaggered grids for hyperbolic conservation laws*, SIAM J. Numer. Anal., 35 (1998), pp. 2147–2168.
[13] G.-S. Jiang and D. Peng, *Weighted ENO schemes for Hamilton–Jacobi equations*, SIAM J. Sci. Comput., 21 (2000), pp. 2126–2143.
[14] G.-S. Jiang and C.-W. Shu, *Efficient implementation of weighted ENO schemes*, J. Comput. Phys., 126 (1996), pp. 202–228.
[15] G.-S. Jiang and E. Tadmor, *Nonoscillatory central schemes for multidimensional hyperbolic conservation laws*, SIAM J. Sci. Comput., 19 (1998), pp. 1892–1917.
[16] S. Jin and Z. Xin, *Numerical passage from systems of conservation laws to Hamilton–Jacobi equations, and relaxation schemes*, SIAM J. Numer. Anal., 35 (1998), pp. 2385–2404.
[17] A. Kurganov and D. Levy, *A third-order semidiscrete scheme for conservation laws and convection-diffusion equations*, SIAM J. Sci. Comput., 22 (2000), pp. 1461–1488.
[18] A. Kurganov, S. Noelle, and G. Petrova, *Semidiscrete central-upwind schemes for hyperbolic conservation laws and Hamilton–Jacobi equations*, SIAM J. Sci. Comput., 23 (2001), pp. 707–740.
[19] A. Kurganov and E. Tadmor, *New high-resolution semi-discrete central schemes for Hamilton-Jacobi equations*, J. Comput. Phys., 160 (2000), pp. 720–724.
[20] A. Kurganov and E. Tadmor, *New high-resolution central schemes for nonlinear conservation laws and convection-diffusion equations*, J. Comput. Phys., 160 (2000), pp. 241–282.
[21] P. D. Lax, *Weak solutions of nonlinear hyperbolic equations and their numerical computation*, Comm. Pure Appl. Math., 7 (1954), pp. 159–193.
[22] B. van Leer, *Towards the ultimate conservative difference scheme*, V. *A second-order sequel to Godunov's method*, J. Comput. Phys., 32 (1979), pp. 101–136.
[23] O. Lepsky, C. Hu, and C.-W. Shu, *Analysis of the discontinuous Galerkin method for Hamilton-Jacobi equations*, Appl. Numer. Math., 33 (2000), pp. 423–434.
[24] D. Levy, G. Puppo, and G. Russo, *Central WENO schemes for hyperbolic systems of conservation laws*, Math. Model. Numer. Anal., 33 (1999), pp. 547–571.
[25] D. Levy, G. Puppo, and G. Russo, *Compact central WENO schemes for multidimensional conservation laws*, SIAM J. Sci. Comput., 22 (2000), pp. 656–672.
[26] P. L. Lions, *Generalized Solutions of Hamilton-Jacobi Equations*, Pitman, London, 1982.
[27] P. L. Lions and P. E. Souganidis, *Convergence of MUSCL and filtered schemes for scalar conservation laws and Hamilton-Jacobi equations*, Numer. Math., 69 (1995), pp. 441–470.
[28] X.-D. Liu and S. Osher, *Nonoscillatory high order accurate self-similar maximum principle satisfying shock capturing schemes* I, SIAM J. Numer. Anal., 33 (1996), pp. 760–779.
[29] X.-D. Liu and E. Tadmor, *Third order nonoscillatory central scheme for hyperbolic conservation laws*, Numer. Math., 79 (1998), pp. 397–425.
[30] C.-T. Lin and E. Tadmor, *L^1-stability and error estimates for approximate Hamilton-Jacobi solutions*, Numer. Math., 87 (2001), pp. 701–735.
[31] C.-T. Lin and E. Tadmor, *High-resolution nonoscillatory central schemes for Hamilton–Jacobi equations*, SIAM J. Sci. Comput., 21 (2000), pp. 2163–2186.
[32] H. Nessyahu and E. Tadmor, *Non-oscillatory central differencing for hyperbolic conservation laws*, J. Comput. Phys., 87 (1990), pp. 408–463.
[33] S. Osher and J. Sethian, *Fronts propagating with curvature dependent speed: Algorithms based on Hamilton-Jacobi formulations*, J. Comput. Phys., 79 (1988), pp. 12–49.
[34] S. Osher and C.-W. Shu, *High-order essentially nonoscillatory schemes for Hamilton–Jacobi equations*, SIAM J. Numer. Anal., 28 (1991), pp. 907–922.

[35] C.-W. Shu, *Essentially non-oscillatory and weighted essentially non-oscillatory schemes for hyperbolic conservation laws*, in Advanced Numerical Approximation of Nonlinear Hyperbolic Equations, Lecture Notes in Math. 1697, A. Quarteroni, ed., Springer, Berlin, 1998, pp. 325–432.
[36] C.-W. Shu and S. Osher, *Efficient implementation of essentially non-oscillatory shock-capturing schemes*, II, J. Comput. Phys., 83 (1989), pp. 32–78.
[37] P. E. Souganidis, *Approximation schemes for viscosity solutions of Hamilton-Jacobi equations*, J. Differential Equations, 59 (1985), pp. 1–43.
[38] P. K. Sweby, *High resolution schemes using flux limiters for hyperbolic conservation laws*, SIAM J. Numer. Anal., 21 (1984), pp. 995–1011.
[39] Y.-T. Zhang and C.-W. Shu, *High-order WENO schemes for Hamilton–Jacobi equations on triangular meshes*, SIAM J. Sci. Comput., 24 (2003), pp. 1005–1030.